02

Spectral and Luminescent Properties of Yb^{3+} in $CCl_4-GaCl_3-Yb^{3+}$ Solutions

© E.A. Seregina, A.A. Seregin, G.V. Tikhonov, A.V. Podkopaev

State Scientific Centre of the Russian Federation Leypunsky Institute for Physics and Power Engineering, Obninsk, Russia

e-mail: seregina@ippe.ru

Received April 12, 2022
Revised November 30, 2022
Accepted February 17, 2023

The absorption and luminescence spectra and the luminescence lifetime of the excited state $^2F_{5/2}$ of Yb^{3+} ions in $CCl_4-GaCl_3-Yb^{3+}$ solutions have been measured. Information was obtained on the Stark splitting of levels, on the absorption and stimulated emission cross sections, and on the quantum yield of Yb^{3+} luminescence. The spectral dependences of the gain cross section are calculated for different relative inverse populations of the $^2F_{5/2}$ excited state. Based on an analysis of the spectral and laser properties of Yb^{3+}, it was concluded that the use of $CCl_4-GaCl_3-Yb^{3+}$ solutions as the active medium of a liquid ytterbium laser is promising

Keywords: carbon tetrachloride, ytterbium, absorption, luminescence, lifetimes, Stark splitting, gain cross section.

DOI: 10.61011/EOS.2023.03.56180.3532-22

Introduction

In the design and operation of high-power, kilowatt-class solid-state lasers, it is essential to arrange for effective cooling of the active medium, which greatly complicates the laser design and limits its capabilities [1]. In contrast to solid-state laser matrices, the use of inorganic laser liquids (ILL's) as an active medium allows the creation of laser elements of large volume with a high activator density and significantly improves the heat dissipation efficiency by circulating the active medium through the resonant cavity. Liquid laser media are cheaper than solid-state matrices, elements of almost any necessary shapes and dimensions can be made from them. However, liquid media have a higher thermo-optic constant than solid media and consequently a higher angular divergence of the laser light [2]. Longitudinal diode pumping [3–5] methods have been developed to reduce the radiation divergence of condensed matter lasers. These methods are particularly relevant for liquid laser media and for creating high-power, high-energy pumping laser systems [6–8] on their basis.

In terms of thermal load reduction, laser media activated by trivalent ytterbium ions (Yb^{3+}) are more promising than the most common neodymium materials [9]. Indeed, compared to Nd^{3+}ions, Yb^{3+} ions have a substantially (in ~ 5 fold) smaller difference between the energies of the pumping and generation quanta.

Separate information on the spectral-luminescent properties of Yb^{3+} in ILL can be found in the papers of I.M. Batyaev and his collaborators [10–13]. Nevertheless, the increased interest in laser liquids and the apparent lack of information prompted us to start paper on the synthesis and investigation of the properties of Yb^{3+} in aprotonic inorganic solvents [14]. The results of the spectral luminescent properties of Yb^{3+} are published for solutions $POCl_3-ZrCl_4-Yb^{3+}$ [15], $SOCl_2-GaCl_3-Yb^{3+}$ [16] and $SO_2Cl_2-GaCl_3-Yb^{3+}$ [17]. These papers give the data on absorption cross-sections, emission and amplification of Yb^{3+}, on luminescence quantum yields, on the Stark splitting of the top $^4F_{5/2}$ and ground $^4F_{7/2}$ states of Yb^{3+}, show the prospects for using these solutions as active media of diode-pumped liquid lasers. It should be noted that the investigated ILL differ in complexity of synthesis, toxicity, corrosivity and physical properties [14,18–20]. Of the known ILL, the least toxic and aggressive are the solutions based on CCl_4-GaCl_3 [19,20]. In contrast to inorganic aprotonic solvents, carbon tetrachloride consists of non-polar molecules and has a very low dielectric constant. The addition of the strong electron acceptor $GaCl_3$ to carbon tetrachloride has created a Nd^{3+} [20] activated laser fluid. In paper [20], the spectral luminescent and generative properties of $CCl_4-GaCl_3-Nd^{3+}$ are given, with the low solubility of neodymium salts ($[Nd^{3+}] < 0.05$ mol/l) noted. Here, it is important to note that the solubility of ytterbium compounds in binary aprotonic inorganic solvents is generally noticeably less than that of neodymium [14] compounds.

The aim of this paper is to create low-toxic ytterbium-containing liquid media for diode-pumped lasers. It was necessary to develop a synthesis technique and prepare solutions $CCl_4-GaCl_3-Yb^{3+}$ with the required parameters, namely with activator concentration $[Yb^{3+}] \geq 0.1$ mol/l, with luminescence quantum yield $\eta > 0.5$ and with inactive loss less 10^{-2} cm^{-1}.

Experiment

To prepare the aprotonic solvent CCl_4-GaCl_3, carbon tetrachloride, CCl_4, qualification „ACS OP-3“, additionally purified by double distillation, gallium(III) chloride,

$GaCl_3$, 99.999%, „LANHIT" were used. Ytterbium(III) compounds were prepared from oxide, Yb_2O_3, 99.999%, „LANHIT". More than 20 solutions $CCl_4-GaCl_3-Yb^{3+}$ with Yb^{3+} concentrations from 0.05 to 0.3 mol/l were prepared by the developed method.

Ready solutions were filled in special spectrometric cuvettes via branch pipes, soldered for sample sealing and subsequent studies. Hellma optical quartz cuvettes with optical layer thicknesses of 0.2, 0.5 or 1.0 cm were used depending on Yb^{3+} concentration and planned experiments.

The spectral-luminescent characteristics of solutions $CCl_4-GaCl_3-Yb^{3+}$ were measured at constant temperature $T = 293 \pm 1$ K. Absorption spectra were recorded with a CARY 500 spectrophotometer in the optical density mode at 850–1200 nm. To account for the influence of the cuvettes on the absorbance measurement results, the same solution was poured into cuvettes of different thicknesses and a differential method was used to process the measurement results. This made it possible to estimate inactive light loss in the $1.1 < \lambda < 1.2\,\mu$m area, where there is no intrinsic absorption Yb^{3+}.

Luminescence spectra and lifetime of τ_{lum} excited state $^2F_{5/2}$ ions Yb^{3+} were measured on a PTI QuantaMaster 8000 spectrofluorimeter. When measuring the luminescence spectra, a continuous light source — xenon lamp OB-75X Arc was used to excite Yb^{3+}. To measure τ_{lum}, Yb^{3+} ions were excited with a pulsed xenon lamp with pulse duration 2 μs and frequency 200 Hz. In both cases, Yb^{3+} was excited by light with a wavelength of $\lambda = 943 \pm 1$ nm. Luminescence spectra were measured in the wavelength range of 945–1200 nm. Luminescence decay kinetics were measured at $\lambda = 1004 \pm 5$ nm. Spectrofluorimeter operation was controlled using FelixGX 4.2.2. For a more detailed description of the measurement methodology, see paper [17].

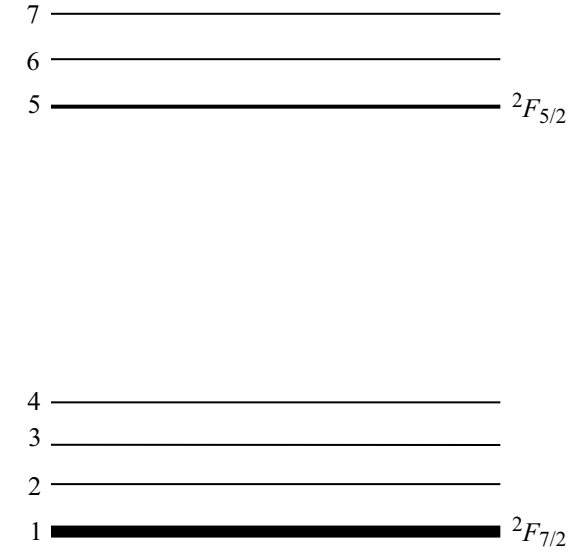

Figure 1. Schematic structure of Yb^{3+} levels in condensed media.

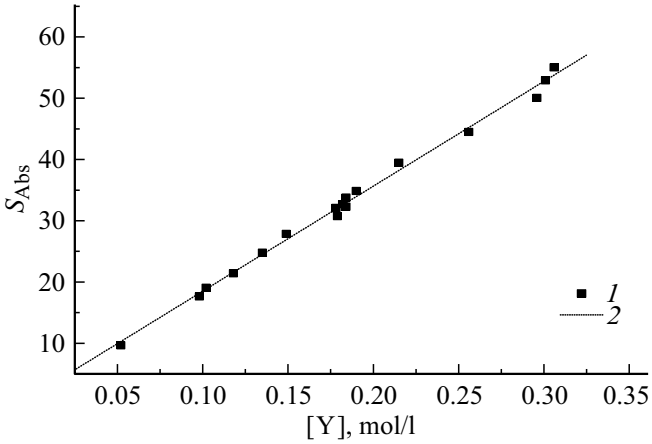

Figure 2. Dependence of absorption band area Yb^{3+} in solutions $CCl_4-GaCl_3-Yb^{3+}$ on concentration Yb^{3+}. *1* — experiment, *2* — linear approximation.

Results and discussion

Trivalent ytterbium ions have a simple energy level scheme — just two states: ground $^2F_{7/2}$ and excited $^2F_{5/2}$, which ensures that there is no energy loss for absorption from the excited state and for up-conversion [9]. In solutions, under the influence of the intramolecular field (ligand field), the main $^2F_{7/2}$ and the excited $^2F_{5/2}$ states of Yb^{3+} into Stark sublevels split, which are schematically shown in Fig. 1.

The absorption spectra are due to transitions between the Stark sublevels of the ground $^2F_{7/2}$ and excited $^2F_{5/2}$ states (Fig. 1). The intensity of light absorption in solutions $CCl_4-GaCl_3-Yb^{3+}$ was proportional to the concentration of Yb^{3+} (Fig. 2). The absorption band intensities were determined by summing the spectra over the wavelengths in the 900–1100 nm area. For the best samples, the inactive losses in the 1.1–1.2 μm area, which were smaller than $5 \cdot 10^{-3}$ cm^{-1}, were estimated.

Fig. 3 shows typical Yb^{3+} absorption spectra in solutions $CCl_4-GaCl_3-Yb^{3+}$. In the presented concentration range of 0.05–0.20 mol/l, the absorption spectra of Yb^{3+} were close in shape. The highest absorption values at $\lambda_m = 981.0$ nm corresponded to the transition $1 \rightarrow 5$ (Fig. 1). This transition determines the energy of the lower Stark sublevel 5 state $^2F_{5/2}$ with $\nu_5 = 10194$ cm^{-1}. The second most intense maximum at $\lambda = 943.6 \pm 0.2$ nm can be attributed to the transition $1 \rightarrow 7$ with the highest energy $\nu_7 = 10598 \pm 3$ cm^{-1}. Fig. 3 clearly shows that the absorption bands associated with the transitions between the remaining sublevels are weakly pronounced.

Typically, mathematical processing [21] methods are used to identify such spectra. Using a priori information about the spectrum and the spectrum differentiation method, the number of bands and their position can be assessed. Knowing this information, the experimental spectrum can

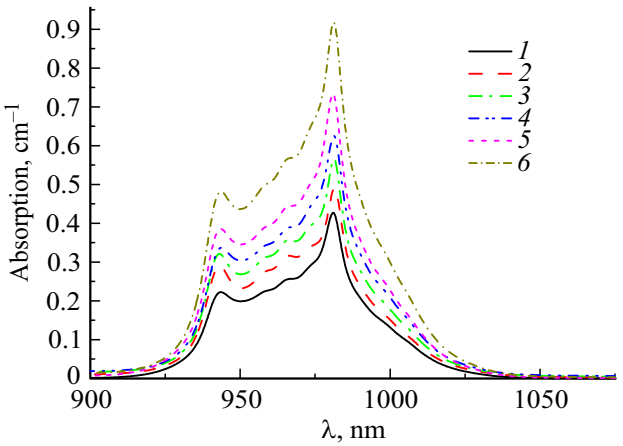

Figure 3. Absorption spectra of Yb^{3+} in solutions $CCl_4-GaCl_3-Yb^{3+}$ with $[Yb^{3+}]$: 0.102 (*1*), 0.118 (*2*), 0.135 (*3*), 0.149 (*4*), 0.178 (*5*) and 0.215 (*6*) mol/l.

Table 1. Parameters of the Lorentz functions that best describe the absorption spectra Yb^{3+} in $CCl_4-GaCl_3-Yb^{3+}$

Transitions between sub-levels of states $^2F_{7/2} \rightarrow {}^2F_{5/2}$	Parameters			
	λ_c, nm	$\Delta\lambda$, nm	ν_c, cm^{-1}	$\Delta\nu$, cm^{-1}
1 → 7	943.1	10.8	10604	121
2 → 7	954.2	14.0	10479	154
1 → 6	964.3	13.4	10370	143
2 → 6	972.9	10.6	10278	112
1 → 5	981.1	9.2	10193	96
2 → 5	991.4	14.7	10087	150
3 → 5	1003.0	16.0	9970	159

be modelled with a set of overlapping Gaussians or Lorentzians and then, the discrepancy between the model and experimental spectra can be minimized. This operation allows the position and width of the absorption bands to be determined more accurately. We used these techniques to treat Yb^{3+} spectra in solutions $SOCl_2-GaCl_3-Yb^{3+}$ [16] and in the present paper.

Fig. 4 shows the results of the Yb^{3+} absorption spectrum in solutions $CCl_4-GaCl_3-Yb^{3+}$. Double differentiation of the spectrum revealed the position of at least seven absorption bands Yb^{3+}, which can be identified as transitions from sub-levels 1 and 2 to sub-levels 5, 6, 7 of the excited state $^2F_{5/2}$ (Fig. 4, *a*). The seventh lane corresponds to the transition from sublevel 3 to sublevel 5. To clarify the position of the weakly expressed maxima and to obtain information about the width of the absorption bands, the spectrum was approximated by a linear combination of the

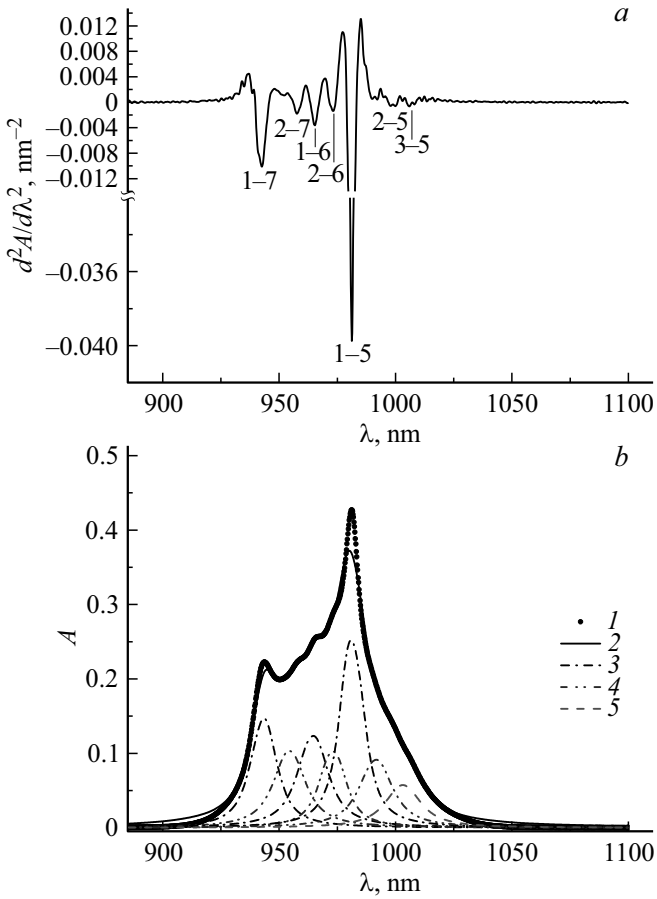

Figure 4. Double differentiated absorption spectrum Yb^{3+} in $CCl_4-GaCl_3-Yb^{3+}$ (*a*). Lorentzian absorption spectrum approximation (*b*): *1* — experimental data; *2* — the sum of the Lorentzian decompositions; *3* — Lorentzians corresponding to electronic transitions from sublevel 1 to Stark sublevels 5, 6, 7; *4* — Lorentzians corresponding to transitions from sub-level 2 to sub-sub-levels 5, 6, 7; *5* – -transitions from sub-level, 3 to sub-level 5.

Lorentz functions, using the expression

$$A(\lambda) = \frac{2B}{\pi} \frac{\Delta\lambda}{4(\lambda - \lambda_c)^2 + \Delta\lambda^2}.$$

Here, B — area under the decomposition line, λ_c — wavelength at distribution maximum, $\Delta\lambda$ — dispersion. The approximation results are shown in Fig. 4, *b* and Table 1. In Table 1, the absorption bands and their dispersions corresponding to transitions from ground state sub-levels $^2F_{7/2}$ to excited state sub-levels $^2F_{5/2}$ are presented not only as functions of λ in nm, but also as functions of ν in cm^{-1}; ν_c — the energy at the absorption band intensity maximum corresponds to the energy of the Stark sub-levels, and $\Delta\nu$ — the band dispersion in cm^{-1}.

The Yb^{3+} absorption spectra in solutions $CCl_4-GaCl_3-Yb^{3+}$ measured in the $A(\lambda)$ absorbance mode were used to calculate the spectral dependence of the $\sigma_a(\lambda)$ absorption cross section. $\sigma_a(\lambda)$ and $A(\lambda)$ are

related by the ratio

$$\sigma_a(\lambda) = \ln 10\, A(\lambda)/lN_t, \qquad (1)$$

where l — optical path length, cm; N_t — concentration Yb^{3+}, cm^{-3}. The largest absorption cross-section Yb^{3+} in solutions $CCl_4-GaCl_3-Yb^{3+}$ was $1.63 \cdot 10^{-20}\,cm^2$ at wavelength 981 nm, which corresponds to light absorption with energy $10194\,cm^{-1}$ and is due to the transition $1 \rightarrow 5$ between the lower Stark sub-levels of the ground $^2F_{7/2}$ and excited $^2F_{5/2}$ states, respectively (Fig. 1). The spectral dependencies $\sigma_a(\lambda)$ Yb^{3+} for all solutions $CCl_4-GaCl_3-Yb^{3+}$ coincided within experimental errors, ±5%.

The $\sigma_a(\lambda)$ Yb^{3+} information was used to calculate the radiative lifetime τ_{rad} of the excited state $^2F_{5/2}$ of Yb^{3+} ions according to the expression [22]

$$1/\tau_{rad} = A_{if} = \frac{g_f}{g_i}\frac{8\pi n^2 c}{\lambda_0^4}\int \sigma_{fi}(\lambda)d\lambda, \qquad (2)$$

where A_{if} — probability of spontaneous emission; g_i and g_f — the degeneracies of the initial and final states of Yb^{3+} ($g_f = 4$ for $^2F_{7/2}$ and $g_i = 3$ for $^2F_{5/2}$); $n = 1.47$ — refraction index; $c = 3 \cdot 10^{10}$ — speed of light, cm/s; λ_0 — wavelength corresponding to the absorption band intensity maximum, cm; $\sigma_{fi}(\lambda)$ — wavelength light absorption cross section λ, cm^2. In the result of the calculations, the average value of τ_{rad} was $624 \pm 30\,\mu s$.

The kinetics of Yb^{3+} luminescence decay in $CCl_4-GaCl_3-Yb^{3+}$ solutions obeyed the exponential law

$$I(t) = I(0)\exp(t/\tau_{lum}),$$

where $I(0)$ — the luminescence intensity amplitude at the initial time, τ_{lum} — the lifetime of the excited state $^2F_{5/2}$. Fig. 5 shows typical Yb^{3+} luminescence decay curves in $CCl_4-GaCl_3-Yb^{3+}$ solutions on a logarithmic scale. It should be noted that at $[Yb^{3+}] < 0.2$ mol/l in cuvettes with $l \le 0.5$ cm radiation reabsorption Yb^{3+}had almost no effect on the τ_{lum} value as well as in solutions $SOCl_2-GaCl_3-Yb^{3+}$ [16] and $SO_2Cl_2-GaCl_3-Yb^{3+}$ [17]. At higher Yb^{3+} concentrations and greater sample thicknesses, light over-absorption may result in an overestimation of τ_{lum}. In such cases, thinner cuvettes should be used or a correction for light over-absorption should be made [23].

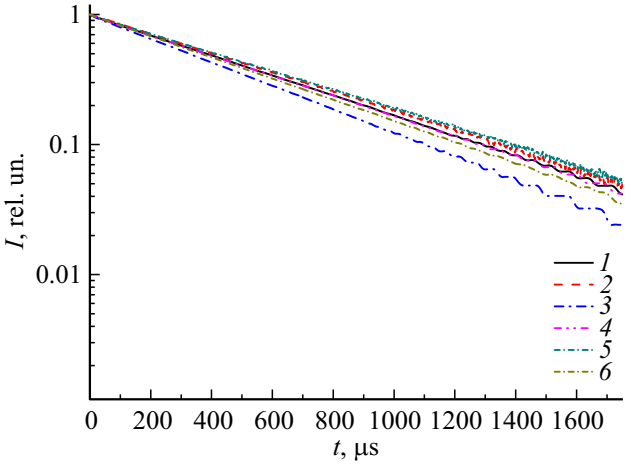

Figure 5. Normalized at $I(0) = 1$ time dependences of luminescence intensity during pulse excitation of solutions $CCl_4-GaCl_3-Yb^{3+}$; $[Yb^{3+}]$: 0.052 (*1*), 0.102 (*2*), 0.118 (*3*), 0.149 (*4*), 0.178 (*5*), 0.214 (*6*) mol/l.

Table 2. Concentrations, τ_{lum} and η Yb^{3+} in sample solutions CCl− GaCl $_3-Yb^{3+}$

№	[Yb], mol/l	$N_{Yb} \cdot 10^{-20}$, cm^{-3}	τ_{lum}, μs	η
1	0.052	0.313	565	0.90
2	0.098	0.590	610	0.97
3	0.102	0.614	584	0.93
4	0.118	0.711	480	0.77
5	0.135	0.813	457	0.73
6	0.149	0.897	562	0.90
7	0.178	1.072	611	0.98
8	0.179	1.078	620	0.99
9	0.182	1.096	618	0.99
10	0.184	1.108	590	0.94
11	0.214	1.288	532	0.85
12	0.256	1.542	606	0.96
13	0.296	1.783	450	0.72
14	0.301	1.813	615	0.98
15	0.306	1.843	397	0.64

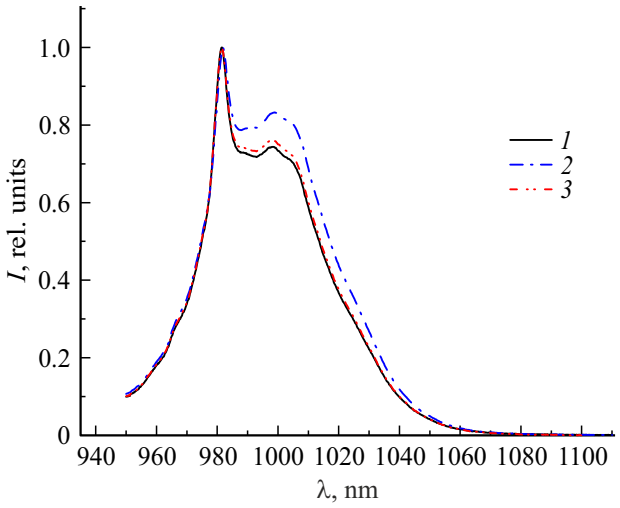

Figure 6. Yb^{3+} luminescence spectra in solutions $CCl_4-GaCl_3-Yb^{3+}$. $[Yb^{3+}] = 0.102$ (*1*) and 0.179 (*2, 3*) mol/l; without correction (*2*) and with reabsorption correction (*3*); $l = 0.2$ cm.

Using the measured τ_{lum} and the $\tau_{rad} = 624\,\mu s$ value, the luminescence quantum yield $\eta = \tau_{lum}/\tau_{rad}$ for Yb^{3+} in prepared solutions $CCl_4-GaCl_3-Yb^{3+}$ was obtained. The results obtained for high quality samples with stable characteristics are presented in Table 2. As can be seen in the Table, $\eta \ge 0.9$ in most samples, as in other known ytterbium-containing ILL [14–17,24].

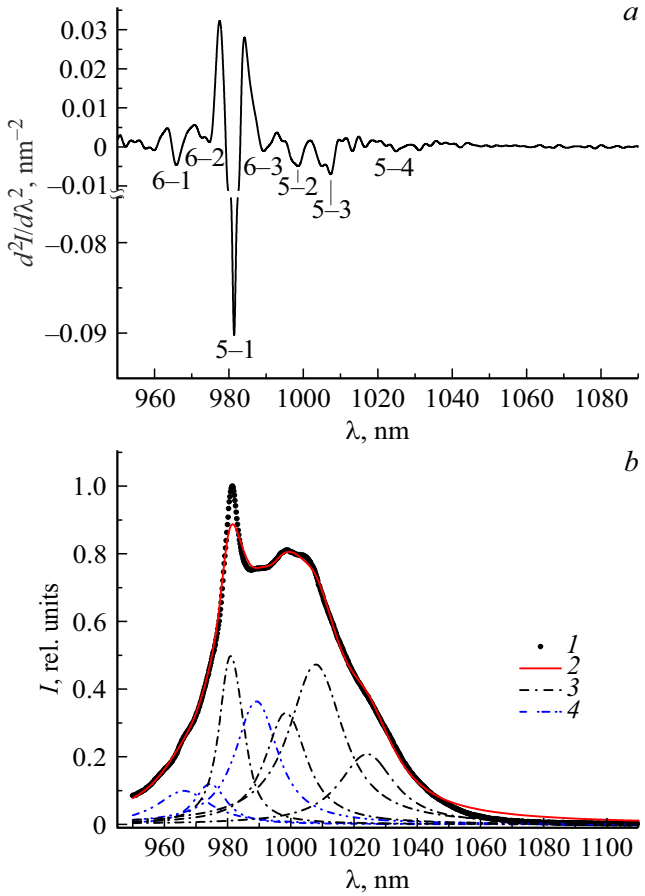

Figure 7. Double differentiated luminescence spectrum (a) and luminescence spectrum Yb^{3+} in solutions $CCl_4-GaCl_3-Yb^{3+}$ (b): *1* — experimental data; *2* — summary of the Lorentzian decomposition; *3* — Lorentzians corresponding to electronic transitions from sublevels 5 to Stark sublevels 1, 2, 3, 4; *4* — Lorentzians corresponding to electronic transitions from sublevels, 6 to Stark sublevels 1, 2, 3.

Luminescence spectra of $CCl_4-GaCl_3-Yb^{3+}$ solutions with different concentrations of Yb^{3+}, corrected for the spectral sensitivity of the recording equipment, are shown in Fig. 6. Unlike the absorption spectra, the shape of the luminescence spectra depends on concentration Yb^{3+}. It is most likely that the differences in the spectra shape are due to the luminescence reabsorption effect proportional to the absorption coefficient Yb^{3+} in solution and leads to an underestimation of the luminescence intensity above all at the maximum intensity at $\lambda = 981.6$ nm. The effect of reabsorption on $I_{\text{lum}}(\lambda)$ was accounted for by introducing a correction for intrinsic absorption. For solutions with $[Yb^{3+}] \leq 0.1$ mol/l and $l \leq 0.2$ cm the reabsorption effect was negligible and had little effect on the shape of the Yb^{3+} luminescence spectra in $CCl_4-GaCl_3-Yb^{3+}$.

The intensity of the $I_{\text{lum}}(\lambda)$ luminescence spectra is due to electronic transitions of Yb^{3+} from the excited state $^2F_{5/2}$ to Stark sublevels of the ground state $^2F_{7/2}$. The luminescence maximum at $\lambda = 981.6$ nm is related to the transition $5 \rightarrow 1$

Table 3. Parameters of the Lorentz functions that best describe the luminescence spectra Yb^{3+} in $CCl_4-GaCl_3-Yb^{3+}$

Transitions between sub-levels of states $^2F_{7/2} \rightarrow {}^2F_{5/2}$	Parameters			
	λ_c, nm	$\Delta\lambda$, nm	ν_c, cm^{-1}	$\Delta\nu$, cm^{-1}
$6 \rightarrow 1$	966.2	19.3	10350	207
$6 \rightarrow 2$	974.5	10.2	10261	107.4
$5 \rightarrow 1$	981.3	6.7	10190	70
$6 \rightarrow 3$	989.2	14.6	10109	149.2
$5 \rightarrow 2$	998.5	14.3	10015	143
$5 \rightarrow 3$	1008.0	19.4	9920	191
$5 \rightarrow 4$	1024.1	19.9	9765	190

Table 4. Energy and relative populations of the ground $^2F_{7/2}$ and excited $^2F_{5/2}$ sublevels Yb^{3+} states in $CCl_4-GaCl_3-Yb^{3+}$

Energy levels Yb^{3+}	Stark sub-levels	$CCl_4-GaCl_3-Yb^{3+}$	
		ν_i, cm^{-1}	N_i/N_t
$^2F_{7/2}$	1	3	$5.5 \cdot 10^{-1}$
	2	178	$2.3 \cdot 10^{-1}$
	3	273	$1.5 \cdot 10^{-1}$
	4	428	$6.8 \cdot 10^{-2}$
$^2F_{5/2}$	5	10193	$1.0 \cdot 10^{-22}$
	6	10370	$4.3 \cdot 10^{-23}$
	7	10604	$1.4 \cdot 10^{-23}$

between the Stark sub-levels of the excited $^2F_{5/2}$ and the ground $^2F_{7/2}$ states. The transitions between the other sublevels are weakly pronounced (Fig. 6). Double differentiation and approximation of the luminescence spectrum by Lorentzians were used to identify the emission transitions between the Stark sub-levels of the excited $^2F_{5/2}$ and the ground $^2F_{7/2}$ states. Fig. 7 shows the results of the Yb^{3+} luminescence spectrum in solutions $CCl_4-GaCl_3-Yb^{3+}$. Double spectrum differentiation revealed the position of at least seven luminescence bands, which can be ascribed to transitions from sublevel 5 to sublevels 1, 2, 3, 4 and from sublevel 6 to sublevel 1, 2, 3 of the ground state $^2F_{7/2}$ (Fig. 7, a). Fig. 7, b and Table 3 show the results of approximating a typical Yb^{3+} luminescence spectrum in solution $CCl_4-GaCl_3-Yb^{3+}$. Table 3 gives the Lorentzian parameters, the sum of which best simulates the luminescence spectrum Yb^{3+}. The positions of the Lorentzian maxima λ_c and their dispersion $\Delta\lambda$ are presented as functions of wavelengths λ in nm and as functions of photon energies ν in cm^{-1}.

Knowing the luminescence photon energy (Table 3) and the energy of the 5 upper excited state sublevel $^2F_{5/2}$ (Table 1), we determined the position of the Stark sublevels of the ground state Yb^{3+} (Table 4). Given that the thermodynamically equilibrium distribution of the populations of the sublevels depends on the medium temperature and the

sublevel energy, we calculated the populations of the Stark sublevels Yb^{3+} as

$$N_i = N_t d_i \exp(-\Delta\nu_i/kT) \Big/ \sum_{i=1}^{7} d_i \exp(\Delta\nu_i/kT),$$

where N_t — concentration Yb^{3+} in $1\,cm^{-3}$ of the solution; d_i — degeneracy by the projection of the angular momentum of the i-th sublevel; $\Delta\nu_i = \nu_i - \nu_1$ — energy difference between i-th sublevel and the 1 ground state sublevel $^2F_{7/2}$; where $k = 0.695$ — Boltzmann constant $cm^{-1} \cdot K^{-1}$; T — ambient temperature, K. For all sub-levels Yb^{3+} $d_i = 2$. Table 4 shows that under thermodynamic equilibrium conditions at room temperature the population of the 1 sublevel of the $^2F_{7/2}$ state is slightly more than half N_t, with the remainder distributed over the Stark sublevels 2–4. Even at sublevel 4, the relative population is $\sim 7\%$. As for the excited state $^2F_{5/2}$, thanks to the large energy gap, the relative populations of the Stark sublevels N_i/N_t $(i = 5, 6, 7)$ are effectively zero $(\leq 10^{-22})$.

Knowing the luminescence spectra, the spectral distribution of the stimulated emission cross section σ_e can be determined in two ways: by the McCumber reciprocity method and using the Fuchtbauer–Ladenburg equation [17,25–27].

The reciprocity method establishes the relation between the cross sections of stimulated emission σ_e and absorption σ_a in terms of energy levels ν_k and their degeneracies on angular momentum projection d_i. The expression for calculating σ_e is as follows :

$$\sigma_e(\nu) = \sigma_a(\nu) \frac{Z_l}{Z_u} \exp\big((\nu_i - \nu_j)/kT\big), \qquad (3)$$

where

$$Z_l = \sum_{i=1}^{4} d_i \exp(-\nu_i/kT), \quad Z_u = \sum_{i=5}^{7} d_i \exp(-\nu_i/kT)$$

— partition function of the lower and upper states, respectively, $d_i = 2$.

The Fuchtbauer–Ladenburg equation allows the spectral dependences of the stimulated emission cross sections $\sigma_e(\lambda)$ to be obtained using known parameters,

$$\sigma_e(\lambda) = \frac{\lambda^5}{8\pi c n^2} \frac{1}{\tau_r} \frac{I(\lambda)}{\int \lambda I(\lambda) d\lambda}. \qquad (4)$$

Here $I(\lambda)$ — luminescence spectrum Yb^{3+} in solution $CCl_4-GaCl_3-Yb^{3+}$ with $[Yb^{3+}] = 0.1$ mol/l (Fig. 4); λ — wavelength at a given point in the spectrum, cm; $n = 1.47$ — the refraction index of the solution; $\tau_{rad} = 6.24 \cdot 10^{-4}$ s — radiative lifetime of excited state $^2F_{5/2}$ ions Yb^{3+}; $c = 3 \cdot 10^{10}$ cm/s — speed of light. The results of calculations of $\sigma_e(\lambda)$ Yb^{3+}using the formulas (3) and (4) and the spectral dependence of the absorption cross section $\sigma_a(\lambda)$ calculated using (1) are shown in Fig. 8. Fig. 8 shows that the results of $\sigma_e(\lambda)$ Yb^{3+} calculations by both methods are in satisfactory agreement. The maximum

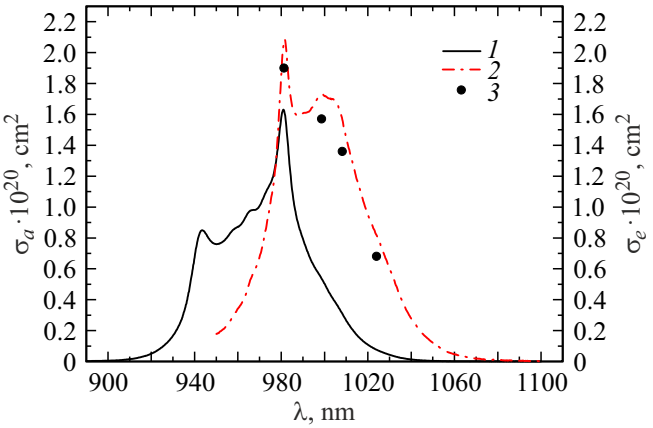

Figure 8. Spectral dependences of absorption cross-sections (*1*) and stimulated emission (*2, 3*) Yb^{3+} in solutions $CCl_4-GaCl_3-Yb^{3+}$; calculations σ_e using the Fuchtbauer–Ladenburg formula (2) and the McCumber reciprocity method (*3*).

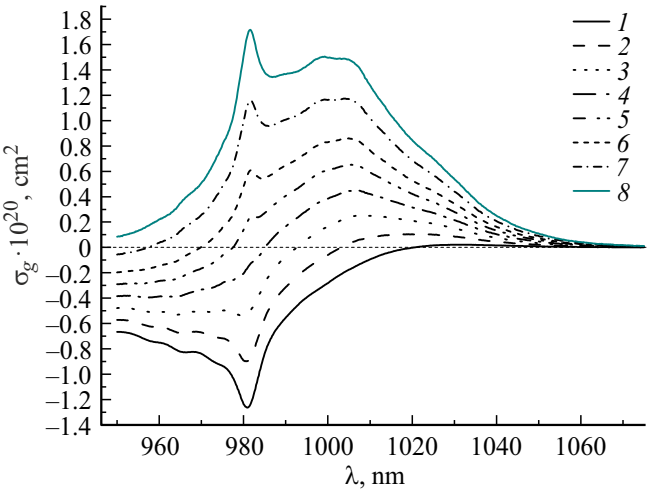

Figure 9. Spectral dependences of the Yb^{3+} gain cross sections in solutions $CCl_4-GaCl_3-Yb^{3+}$ at different values of the relative inverse population β: 0.1 (*1*), 0.2 (*2*), 0.3 (*3*), 0.4 (*4*), 0.5 (*5*), 0.6 (*6*), 0.75 (*7*), 0.9 (*8*).

values of $\sigma_a(\lambda)$ and $\sigma_e(\lambda)$ are registered at wavelength 981.0 ± 1.0 nm and correspond to transitions between Stark sub-levels $1 \rightarrow 5$ and $5 \rightarrow 1$. The overlap of the absorption and stimulated emission cross sections in a wide wavelength area is noteworthy. When the laser medium is excited, this overlapping of the absorption and emission bands results in an increase in the threshold pump energy or even a cessation of generation, depending on the ratio of $\sigma_e(\lambda)$ and $\sigma_a(\lambda)$ at the generation wavelength. Therefore, it is important to obtain gain cross section data $\sigma_g(\lambda)$ Yb^{3+} to quantify the generation characteristics of the active medium $CCl_4-GaCl_3-Yb^{3+}$.

Knowing $\sigma_e(\lambda)$ and $\sigma_a(\lambda)$ Yb^{3+} in solutions $CCl_4-GaCl_3-Yb^{3+}$, we calculated the spectral dependence

Table 5. Maximums of radiation gain cross sections at relative inverse population $\beta = 0.75$ for ytterbium-containing ILL and some solid state media

ILL	λ_1, nm	$\sigma_{g1} \cdot 10^{20}$, cm^2	λ_2, nm	$\sigma_{g2} \cdot 10^{20}$, cm^2
$POCl_3-ZrCl_4-Yb^{3+}$ [15]	977.6	0.844	1004.0	0.560
$SOCl_2-GaCl_3-Yb^{3+}$ [16]	980.5	1.070	1000.5	1.082
$SO_2Cl_2-GaCl_3-Yb^{3+}$ [17]	979.0	1.557	1006.0	0.880
$CCl_4-GaCl_3-Yb^{3+}$	981.6	1.163	1004.0	1.173
Solid media	λ_1, nm	$\sigma_{g1} \cdot 10^{20}$, cm^2	λ_2, nm	$\sigma_{g2} \cdot 10^{20}$, cm^2
$YVO_4:Yb^{3+}$ [28]	982	≈ 1.6	1010.0	≈ 1.9
$KNGG:Yb^{3+}$ [27, p.10–17]	975	≈ 0.65	1030	≈ 0.82
$ZrO_2-Y_2O_3-Yb_2O_3$ [27, p.29–33]	980	≈ 0.25	1006.0	0.880
$CaF_2:Yb^{3+}$ [29]	992	≈ 0.35[1]	1035.0	≈ 0.21[1]
Yb,In:KLuW — $E \parallel N_m$ [30]	981	≈ 3.8[2]	1030	≈ 1.6[2]
Yb,In:KLuW — $E \parallel N_p$ [30]]	981	≈ 0.4[2]	1030	≈ 0.9[2]

[1] $\beta = 0.40$; [2] $\beta = 0.60$.

of the gain cross section $\sigma_g(\lambda)$ Yb^{3+} using the expression [16,17]

$$\sigma_g(\lambda) = \beta[(\sigma_e(\lambda) + \sigma_a(\lambda)] - \sigma_a(\lambda),$$

where $\beta = N_u/N_t$ — relative inverse population; N_u — inverse population of all Stark sub-levels of the excited $^2F_{5/2}$ state during pumping; N_t — concentration Yb^{3+}. The results of calculating the spectral dependences of the gain cross section $\sigma_g(\lambda)$ Yb^{3+} for different values of the relative inverse population β are shown in Fig. 9. With increasing β values $\sigma_g(\lambda)$ increase, and the maximum shifts from $\lambda = 1030$ nm at $\beta = 0.1$ towards lower wavelengths. At $\beta > 0.5$ in the area of the maximum intensity of the stimulated cross section Yb^{3+} at $\lambda \approx 981$ nm another maximum appears in the spectrum $\sigma_g(\lambda)$, which increases with increasing relative inverse population β. Note the smooth change in the wavelength dependence of the gain cross section and the large spectral width of the gain contour $\Delta\sigma_g$, increasing with increasing inverse population from 35 nm at $\beta = 0.3$ to 47 nm at $\beta \geq 0.6$. These properties Yb^{3+} in $CCl_4-GaCl_3-Yb^{3+}$ are important for the development of diode-pumped liquid tunable lasers.

Table 5 shows the values of maximum $\sigma_g(\lambda)$ Yb^{3+} gain cross sections in ILL at the relative inverse population $\beta = 0.75$ and $\sigma_g(\lambda)$ in some ytterbium-containing solid state media. The values of $\sigma_g(\lambda)$ Yb^{3+} maxima in the studied ILL are in the range $0.56 \cdot 10^{-20}-1.56 \cdot 10^{-20}$ cm^2 at $\beta = 0.75$. As can be seen from Table. 5, for the investigated ILL $\sigma_g(\lambda)$ Yb^{3+} are close and even exceed the corresponding $\sigma_g(\lambda)$ values of some solid-state ytterbium-containing media — single crystals [25,28,29], disordered crystals and solid solutions [27,30], ytterbium glasses with high gain [31,32], on which diode pumped generation at Yb^{3+} has been obtained.

Importantly, laser generation at Yb^{3+} in liquid media by longitudinal diode pumping of ILL $SOCl_2-GaCl_3-Yb^{3+}$, $SO_2Cl_2-GaCl_3-Yb^{3+}$ and $POCl_3-SnCl_4-Yb^{3+}$ [33] has recently been obtained for the first time.

Large values of $\sigma_g(\lambda)$ and η, stability of spectral-luminescent properties indicate the promising use of $CCl_4-GaCl_3-Yb^{3+}$ solutions as an active medium to create pumped high-energy diode-pumped liquid lasers.

Conclusion

Absorption, luminescence spectra and excited state lifetime Yb^{3+} in solutions $CCl_4-GaCl_3-Yb^{3+}$ were measured. Experimental data on absorption cross sections $\sigma_a(\lambda)$ and stimulated emission cross sections $\sigma_e(\lambda)$ Yb^{3+} were obtained. The maximum values were $\sigma_a = 1.63 \cdot 10^{-20}$ cm^2 at $\lambda = 981.0$ nm and $\sigma_e = 2.08 \cdot 10^{-20}$ cm^2 at $\lambda = 981.6$ nm. For high quality solutions $CCl_4-GaCl_3-Yb^{3+}$, luminescence quantum yield $\eta > 0.9$. The inactive light loss in the $1.1-1.2\,\mu$ m area is $\approx 5 \cdot 10^{-3}$ cm^{-1}.

The spectral dependences of the gain cross section $\sigma_g(\lambda)$ Yb^{3+} for different values of the relative inverse population β of the excited state $^2F_{5/2}$ are calculated. It is found that $\sigma_g(\lambda)$ in $CCl_4-GaCl_3-Yb^{3+}$ depends on the relative inverse population and represents a wide band in the wavelength area from 980 to 1040 nm. At $\beta > 0.7$, the values of the two maxima $\sigma_g(\lambda)$ in $CCl_4-GaCl_3-Yb^{3+}$ are approximately equal and even exceed the corresponding values in ILL where diode-pumped laser radiation generation is obtained.

Thus, the laser liquid $CCl_4-GaCl_3-Yb^{3+}$ can be recommended for use as an active medium in diode pumped lasers in the wavelength area 980–1040 nm.

Acknowledgments

The authors would like to thank J.V. Krivosheev for assistance in measurements.

Funding

The studies were funded by the Russian Foundation for Basic Research and Government of the Kaluga Region (scientific project № 19-43-400004).

Conflict of interest

The authors declare that they have no conflict of interest.

References

[1] I.V. Glukhikh, S.A. Dimakov, R.F. Kurunov, S.S. Polikarpov, S.V. Frolov. ZhTF, **81** (8), 70 (2011). (in Russian).
[2] Y.G. Anikeev, M.E. Zhabotinsky, V.B. Kravchenko. *Lazery na neorganicheskikh zhidkostyakh* (Nauka, M., 1986). (in Russian).
[3] E.R. Ault, B.J. Comaskey, T.C. Kuklo. *High Average Power Laser Using a Transverse Flowing Liquid Host:* U. S. Patent 6600766 B1(2003).
[4] I.I. Kuznetsov, I.B. Mukhin, O.L. Vadimova, O.V. Palashov. Kvant. elektron., **43** (3), 207 (2015). (in Russian).
[5] A.M. Bulkanov, D.A. Nikolaev, V.B. Tsvetkov, A.I. Shamatova, I.A. Shcherbakov. Kvant. elektron., **48**, 5 (468) (2018). (in Russian).
[6] X. Zheng, S. Yi, L. Chunling, L. Mi, X. Xiufang, L. Liqing, W. Yali, Y. Feng, W. Deyong, J. Jianfeng, T. Bo, L(U) Wenqiang. High Power Laser and Particle Beams, **18** (12), 1941 (2006).
[7] X. Zheng, L. Mi, L. Chunling, W. Yali. Acta Optica Sinica, **30** (9), 2620 (2010). DOI: 10.3788/AOS20103009.2620
[8] Li Mi, Wang Yali, Li Chunling, Wang Jiao, Liu Liqing. Acta Optica Sinica, **31** (2), 135 (2011). DOI: 10.3788/AOS20113102.0214004
[9] G. Boulon. J. Alloys and Compounds, **451** (1–2), 1 (2008). DOI: 10.1016/j.jallcom.2007.04.148
[10] I.M. Batyaev, N.V. Danilchuk, Y.A. Kabatsky, V.N. Shapovalov, S.M. Shilov. Zhurn. prikl. spektr., **53** (2), 336 (1990).
[11] I.M. Batyaev, S.Y. Morev. Opt. i spektr., **79** (6), 954 (1995). (in Russian)
[12] Y.A. Kabatsky. *Fiziko-khimicheskiye i generatsionnyye svoystva neorganicheskikh lyuminestsentnykh materialov, aktivirovannykh Nd, Yb, Er.*Avtoref. kand. dis. (RGPI, L., 1990). (in Russian)
[13] S.M. Shilov.*Lyuminestsentno-spektral'nyye svoystva soyedineniy redkozemel'nykh elementov v khloridnykh sistemakh i poristykh sredakh.*Avtoref. dokt. dis. (RGPU, SPb., 2009). (in Russian)
[14] G.V. Tikhonov, A.S. Babkin, E.A. Seregina, A.A. Seregin. Neogranicheskiye materialy **53** (10), 1122 (2017). (in Russian) DOI: 10.7868/S0002337X17100165 [G.V. Tikhonov, A.S. Babkin, E.A. Seregina, A.A. Seregin. Inorganic Materials, **53** (10), 1097 (2017). DOI: 10.1134/S0020168517100168
[15] A.S. Babkin, E.A. Seregina, A.A. Seregin, G.V. Tikhonov. Opt. i spektr., **125** (4), 507 (2018). (in Russian) DOI: 10.21883/OS.2018.10.46703.157-18 [A.S. Babkin, E.A. Seregina, A.A. Seregin, G.V. Tikhonov. Opt. Spectrosc., **125** (4), 528 (2018). DOI: 10.1134/S0030400X18100053].
[16] E.A. Seregina, A.A. Seregin, G.V. Tikhonov. Opt. Spectrosc., **128** (10), 1551 (2020). DOI: 10.1134/ S0030400X20100240.
[17] E.A. Seregina, A.A. Seregin, G.V. Tikhonov. Opt. i spektr., **129** (12), 1484 (2021). (in Russian). DOI: 10.21883/OS.2021.12.51735.1883-21
[18] I.V. Mochalov, N.P. Bondareva, A.S. Bondarev, S.A. Markosov. Kvant. elektron., **9** (5), 1024 (1982). (in Russian).
[19] I.M. Batyaev. JTF, **64** (6), 125 (1994) (in Russian).
[20] I.M. Batyaev, Y.A. Kabatsky. Neorgan. mater, **27** (9), 1928 (1991).(in Russian)
[21] V.S. Sizikov, A.V. Lavrov. Opt. i spectr., **124** (6), 723 (2018). (in Russian). DOI: 1021883/OS.2018.06.46071.28-18
[22] G. Boulon, Y. Guyot, H. Canbano, S. Hraiech, A. Yoshikawa. J. Opt. Soc. Am. B., **25** (5), 884 (2008).
[23] S.V. Kurilchik, V.E. Kisel, N.V. Kudeshov, A.A. Pavlyuk. Pribory i metody izmereniy, **1** (2), 59 (2011). (in Russian).
[24] G.V. Tikhonov, E.A. Seregina.„*Sovremennaya khimicheskaya fizika*". *XXXIII simpozium. Tuapse, 2020. Sborkik tezisov* (Doblest, M., 2020), s. 70–71. (in Russian)
[25] Laura D. DeLoach, Stephen A. Payne, L.L. Chase, Larry K. Smith, Wayne L. Kway, William F. Krupke. IEEE J. Quantum Electron., **29** (4), 1179 (1993).
[26] D.E. McCumber. Phys. Rev., *136* (4a), A954 (1964).
[27] V.E. Shukshin // Trudy IOF im. A.M. Prokhorova RAN, **64** (2008). (in Russian).
[28] Y.K. Voronko, V.V. Kochurikhin, A.A. Sobol, S.N. Ushakov, V.E. Shukshin. Neorgan. mater, **40** (10), 1234 (2004).(in Russian)
[29] Martin Kahle, Jörg Körner, Joachim Hein, Malte C. Kaluza. Optics & Laser Technology, **92**, 19–23 (2017). DOI: 10.1016/j.optlastec.2016.12.025
[30] J.M. Serres, X. Mateos, P. Loiko, U. Griebner, V. Petrov, K. Yumashev, M. Aguiló, F. Díaz. J. Lumin., **183**, 391 (2017). DOI: 10.1016/j.jlumin.2016.11.018
[31] Ju H. Choi, Alfred Margaryan, Ashot Margaryan, Frank G. Shi. J. Alloys and Compounds, **396**, 79 (2005).
[32] Shujiang Liu, Anxian Lu. Hindawi Publishing Corporation Laser Chemistry (2008). ID 656490. DOI: 10.155/2008/656490
[33] I.A. Denezhkin, Y.A. Dyuzhov, O.F. Kukharchuk, E.A. Seregina, V.N. Smolsky, A.A. Suvorov, G.V. Tikhonov.„*Sovremennaya khimicheskaya fizika* ". *XXXIII simpozium. Tuapse, 2021. Sborkik tezisov* (Doblest, M., 2021), s. 306. (in Russian)

Translated by Y.Deineka